Orientational Disorder of C_{60} in Li_2CsC_{60}

Ichiro Hirosawa,* Kosmas Prassides,* Junichiro Mizuki,
Katsumi Tanigaki, Matthew Gevaert, Alexandros Lappas,
Jeremy K. Cockcroft

The x-ray diffraction of the nonsuperconducting ternary fulleride Li_2CsC_{60} reveals at room temperature a face-centered-cubic ($Fm\bar{3}m$) disordered structure that persists to a temperature of 13 Kelvin. The crystal structure is best modeled as containing quasispherical [radius of 3.556(4) angstroms] C_{60}^{3-} ions, in sharp contrast to their orientational state in superconducting face-centered-cubic K_3C_{60} (merohedral disorder) and primitive cubic Na_2CsC_{60} (orientational order). The orientational disorder of the carbon atoms on the C_{60}^{3-} sphere was analyzed with symmetry-adapted spherical-harmonic functions. Excess atomic density is evident in the $\langle 111 \rangle$ directions, indicating strong bonding Li^+–C interactions, not encountered before in any of the superconducting alkali fullerides. The intercalate-carbon interactions and the orientational state of the fullerenes have evidently affected the superconducting pair-binding mechanism in this material.

Superconducting alkali fullerides with a stoichiometry of $A_2A'C_{60}$ (A and A' are alkali metals) can be classified into two distinct families, distinguished through the orientational state adopted by the fulleride C_{60}^{3-} ions in the crystal structure. The fullerides K_3C_{60} [superconducting transition temperature (T_c) ~ 19 K] and Rb_3C_{60} (T_c ~ 29 K) adopt a merohedrally disordered face-centered-cubic (fcc) ($Fm\bar{3}m$) structure in which the C_{60}^{3-} ions are randomly distributed between two orientations related by 90° rotations about the cubic axes (*1*). Na_2CsC_{60} (T_c ~ 12 K) (*2*) and Na_2RbC_{60} (T_c ~ 3.5 K) (*3*) adopt a primitive cubic ($Pa\bar{3}$) structure in which ~88% of the fulleride ions are rotated counterclockwise by ~98° about the appropriate [111] cube diagonal, with the remaining ions adopting minor orientations. Although the pair-binding mechanism in the fullerenes remains to be determined unambiguously, both currently prevailing [electronic (*4*) and electron-phonon coupling (*5*)] models associate it with intramolecular properties. The alkali metals fully donate their electron to the fullerene units and essentially act as simple spacers. The intermolecular separation appears to modulate the electronic density of states at the Fermi level (6) and, within each structural family (*2*), to result in a monotonic increase in T_c with increasing lattice constant. Differences between the two structural families at the same intermolecular separation can be attributed (*2*) to the different orientational state of the C_{60}^{3-} ions and the resulting intermolecular potential that can sensitively affect electron hopping and, as a consequence, the electronic and conducting properties of the solids (*7*). Experimentally, the primitive cubic family of fullerides is evidently characterized by a steeper dependence of T_c on the interfullerene spacing (*2*).

Here, we address the problem of the structural properties of the ternary fulleride Li_2CsC_{60}, containing the smallest and least electropositive alkali metal ion, Li^+ (radius, $r_{Li^+} = 0.60$ Å) in the tetrahedral interstices. Little is known about the structural, conducting, and electronic properties of such Li^+ intercalated fullerides, with Li_2RbC_{60} and Li_2CsC_{60} the only reported stable phases with an $A_2A'C_{60}$ stoichiometry (*8*). We found no evidence in Li_2CsC_{60} for a transition to a superconducting state down to 50 mK, while differential scanning calorimetry (DSC) measurements showed no indication of a structural phase transition between 100 and 450 K. We then probed its structural properties between 13 and 300 K by both laboratory and high-resolution synchrotron x-ray diffraction. Unexpectedly, we found that its crystal structure did not belong to any of the two fulleride structural families known at present; it was fcc ($Fm\bar{3}m$) but with an orientational state for the C_{60}^{3-} ions that were best modeled as quasispherical units of radius 3.556(4) Å. Deviations from perfect sphericity were more pronounced than those encountered in the disordered phase of pristine C_{60} (*9*). A symmetry-adapted spherical-harmonics analysis of the orientational distribution function revealed a substantial excess of carbon atom density in the $\langle 111 \rangle$ directions facing the Li^+ ions. This excess is the signature of a strong stabilizing Li^+–C interaction, unprecedented in fullerene chemistry but reminiscent of many similar bonding situations, encountered in the widespread organometallic chemistry of Li (*10*). Also, the partial hybridization of carbon p_z and metal *s* orbitals has been postulated for the Li intercalation compound of graphite LiC_6 (*11*). Here, we provide an example of a new structural family of ternary fullerides. We associate the absence of superconductivity in this family with the enhanced lithium-carbon interactions and the modified intermolecular potential.

Measurements from x-ray diffraction methods on Li_2CsC_{60} samples (*12*) sealed in thin-wall glass capillaries 0.5 mm in diameter were performed both with a rotating anode (12.5 kW) and a synchrotron radiation source. Laboratory diffraction patterns (Cu $K_{\alpha 1}$ radiation) were recorded between 13 and 300 K. High-resolution x-ray measurements ($\lambda = 0.8717$ Å, $2\theta = 4°$ to 44°) were performed with the sample inside an Oxford Instruments (Bedford, Massachusetts) continuous-flow helium cryostat at 50 and 300 K at the SRS Station 9.1, Daresbury Laboratory, United Kingdom. Data analysis was performed with the PROFIL suite of Rietveld analysis programs (*13*), incorporating symmetry-adapted spherical-harmonic functions for the description of spherically disordered molecules to order 12.

The rotating anode x-ray diffraction profiles could be indexed on an fcc structure at all temperatures. Peaks violating fcc rules did not appear even when an extended scan with a data accumulation rate of 60 s per point was performed at 13 K. Under the same conditions, peaks indexed on a primitive cubic lattice were clearly evident in Na_2CsC_{60} and Na_2RbC_{60}. The results of the DSC measurements are in agreement, showing no indication of a phase transition with latent heat (ΔH) greater than 0.1 J/g in the temperature range 100 to 450 K (Fig. 1). No sign of unreacted C_{60} was evident. Under the same conditions, Na_2CsC_{60} clearly showed an order-disorder transition at 313 K with ΔH ~ 2.7 J/g (Fig. 1) (*14*).

The synchrotron powder diffraction profiles at 50 and 300 K confirmed that the crystal structure of Li_2CsC_{60} was fcc. Rietveld refinements of the profiles were attempted in space group $Fm\bar{3}m$ with the Li^+ and Cs^+ ions occupying the tetrahedral and octahedral holes, respectively. Various possibilities, characterized by the differing orientational states of the C_{60} units, were explored in the refinements of both data sets. The merohedrally disordered C_{60} model that had been found appropriate for the binary fullerides K_3C_{60} and Rb_3C_{60} (*1*) gave poor agreement with the data (weighted profile *R* factor, R_{wp} = 23.3%; intensity *R* factor, R_I = 15.7% at room temperature). Increased disorder of the C_{60} unit was then modeled by placing it at the origin of the unit cell in one of its two standard orienta-

---

I. Hirosawa, J. Mizuki, K. Tanigaki, Fundamental Research Laboratories, NEC Corporation, 34 Miyukigaoka, Tsukuba 305, Japan.
K. Prassides, M. Gevaert, A. Lappas, School of Chemistry and Molecular Sciences, University of Sussex, Brighton BN1 9QJ, UK.
J. K. Cockcroft, Department of Crystallography, Birkbeck College, London WC1E 7HX, UK.

*To whom correspondence should be addressed.

tions and allowing it to rotate counterclockwise about the ⟨111⟩ orientation by an arbitrary angle ϕ. The application of all the symmetry operations of the cubic group O_h to the C_{60} unit generally results in the superposition of eight symmetry-equivalent, differently oriented molecules (*15*). Each fullerene unit is thus modeled by 8 × 60 = 480 points on a sphere, each point occupied with the same probability. Profile refinements were performed after ϕ was varied in a stepwise manner in multiples of 5° between ϕ = 0° and 120°, giving improved agreement with the data, compared to the merohedral model. The lowest *R* factors ($R_{wp} \sim 16.9\%$, $R_I \sim 9.2\%$) were obtained in the vicinity of $\phi \sim 17°$, 59°, and 98°. However, the refinement further improved when each fullerene molecule, instead of being considered to arise from a distribution of distinct carbon atoms, was modeled by a simple spherical shell of electron density ($R_{wp} = 15.4\%$, $R_I = 9.0\%$).

The Rietveld refinement results are thus consistent with pronounced orientational disorder of the fullerene ions. Because the carbon atom motion is necessarily confined to the surface of a sphere, a convenient way of describing the scattering density in such cases is in terms of symmetry-adapted spherical-harmonic (SASH) functions (*16*). The PROFIL Rietveld refinement program (*17*) was extended to include SASH functions to order 12 and then used to fit the Li_2CsC_{60} diffraction data. We take into account the icosahedral symmetry of the C_{60} units and note that they occupy the 4a sites of $m\bar{3}m$ (O_h) symmetry in the fcc lattice. This positioning only necessitates consideration of SASH functions, $K_{l\nu}$, with values for l = 0, 6, 10, and 12, that transform as A_{1g} in O_h (*18*). Refinement was initiated with r = 3.54 Å and C_{01} = 1.0. It proceeded smoothly and resulted in improved agreement factors ($R_{wp} = 14.4\%$, $R_I = 7.6\%$).

However, a different Fourier analysis of the diffraction data revealed that the present model was drastically underestimating the electron density residing in the tetrahedral holes. Thus, we considered a structural model that allowed for disorder of the alkali ions. Unconstrained refinement was robust and rapidly converged to excellent agreement factors (Fig. 2), resulting from partial occupation of the tetrahedral holes by Cs^+ ions. At the final stages, the alkali metal occupancies were constrained to satisfy the stoichiometry of the material, $(Li_{2-x}Cs_x)_{tet}$-$(Li_xCs_{1-x})_{oct}C_{60}$. The variable x refined to 0.115(5), indicating a ~6% occupation of the tetrahedral holes by Cs^+ (R_{wp} = 11.4%, R_I = 5.9%). Refinements of the 50 K data also proceeded routinely with the same structural model, and the fitted parameters at both 50 K and room temperature are summarized in Table 1.

Several points arising from the results of the present refinements are of particular interest. First, the $C_{60}{}^{3-}$ ions remain disordered at all temperatures with a spherical radius of 3.556(4) Å, somewhat larger than the radius of neutral C_{60} [3.5429(6) Å (*9*)] but entirely consistent with the expected effect of reduction. In addition, disorder effects associated with the alkali metal ions in both the tetrahedral and octahedral interstitial sites were identified. Partial occupation (~6%) by the large Cs^+ cations of the small tetrahedral holes seems surprising, especially because the evidence so far on ternary metal fullerides has been strongly in favor of complete order for both sites (*19*). However, the large difference in scattering power between Li and Cs in the present case allowed us to probe the alkali metal distribution with high accuracy. Both the spherical shape of the fulleride ions and the enlarged effective radius of the tetrahedral ions in Li_2CsC_{60} lead to a lattice constant [a = 14.0746(12) Å at room temperature] somewhat larger than expected from a direct extrapolation from the other families of fullerides.

Because the error in the determination of the fitted $C_{l\nu}$ coefficients of the SASH functions (Eq. 4) increases rapidly with increasing order, it was not possible to extract reliable values for higher order coefficients (*20*). Comparing these coefficients (Table 1) with those determined for C_{60} (*9*), we find (i) that they are relatively large and (ii) that their signs and relative magnitudes are reversed. These findings indicate that the deviations from spherical isotropy are more pronounced in the present case, consistent with the more strongly

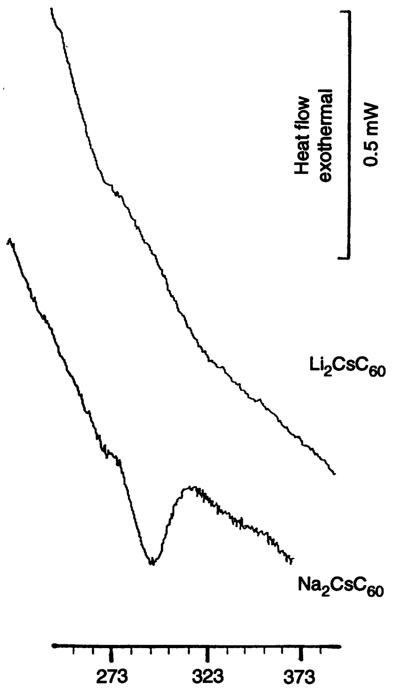

Fig. 1. DSC measurements on powder samples of Li_2CsC_{60} and Na_2CsC_{60}.

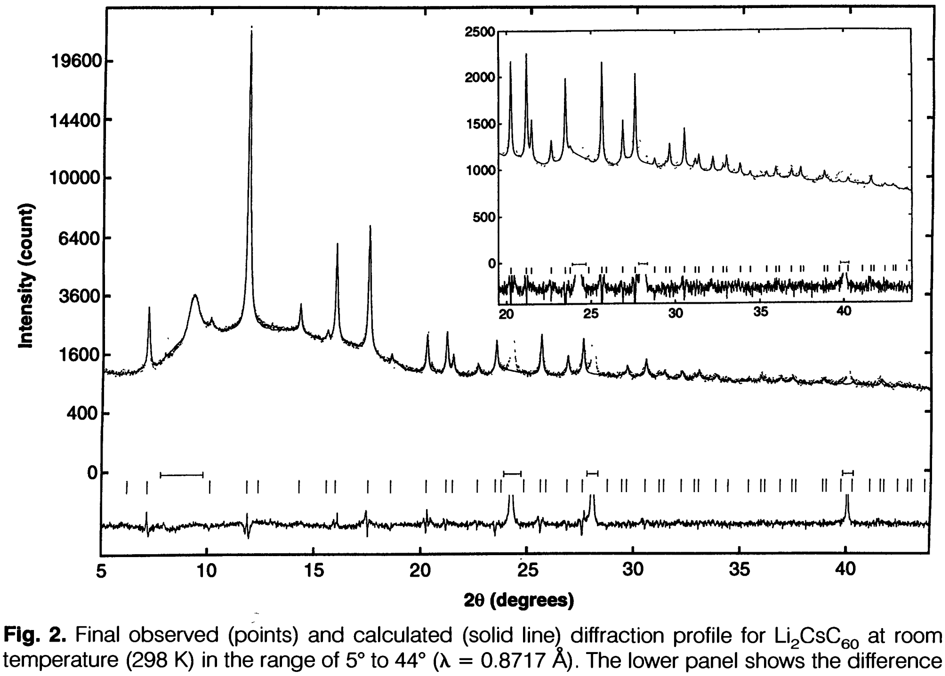

Fig. 2. Final observed (points) and calculated (solid line) diffraction profile for Li_2CsC_{60} at room temperature (298 K) in the range of 5° to 44° (λ = 0.8717 Å). The lower panel shows the difference profile. The normalized intensity is plotted with a square root scale to amplify the weak high-angle peaks. Vertical marks indicate the observed reflections. Three peaks arising from copper reflections from the cryostat and the scattering in the vicinity of ~9° arising from the glass capillary were excluded from the refinement (as indicated by the horizontal lines above the marks). The inset shows in detail an expanded view of the profile in the range of 20° to 44°.

anisotropic crystal field generated by the presence of the alkali ions. In addition, the orientational distribution function is drastically different. From the refined values of the coefficients, we calculated the carbon orientational density function, shown in Fig. 3 as a contour map. The value of $\rho(\mathbf{r})$ is normalized to be equal to one for the isotropic case, with larger and smaller values representing density excess and deficit, respectively. Unlike the rotator phase of pristine C_{60} in which a density deficit is evident in the $\langle 111 \rangle$ directions (*9*), Fig. 3 shows the existence of a density excess along $\langle 111 \rangle$ and a deficit along $\langle 100 \rangle$. This distribution means that the carbon atoms have a high probability of being close to the Li^+ ions that occupy the tetrahedral holes while; at the same time, avoiding the Cs^+ ions located at the octahedral interstices. This result may be understood if a strong interaction with some covalent character exists between the least electropositive, strongly polarizing alkali ion, Li^+, and the fullerene carbon atoms. The $d_{Li-C_{60}}$ distances (2.54 Å at room temperature, 2.50 Å at 50 K) do not indicate, however, large covalent interactions.

Table 1. Refined parameters for Li_2CsC_{60} obtained from Rietveld refinements at room temperature and at 50 K. Estimated errors in the last digits are given in parentheses. The space group is $Fm\bar{3}m$. The x-ray wavelength is 0.8717 Å. The x-ray scattering factors for the neutral atoms were used, and anomalous scattering corrections ($f' = -0.405$, $f'' = 3.036$ electrons per atom) were included for Cs. Unconstrained refinements in the thermal factors of the tetrahedral and octahedral ions showed little difference in their values; these were then constrained to be equal in the final refinement cycles. The R factors are defined as $R_{wp} = \{\Sigma w[y(\text{obs})-y(\text{calc})]^2/\Sigma wy(\text{obs})^2\}^{1/2} \times 100\%$, $R_{exp} = \{(N\text{-}P+C)/\Sigma wy(\text{obs})^2\}^{1/2} \times 100\%$, $R_I = \Sigma|I(\text{obs})-I(\text{calc})|/\Sigma I(\text{obs}) \times 100\%$, where $w = 1/\sigma\, y(\text{obs})^2$. Data for Li_2CsC_{60} at room temperature are as follows: cell constants, 14.0746(12) Å; C_{60} shell radius, 3.556(4) Å; cubic harmonic coefficients, $C_{0,1} = 1.0$, $C_{6,1} = 0.08(1)$, $C_{10,1} = -0.24(4)$; R factors, $R_{wp} = 11.4\%$, $R_{exp} = 4.5\%$, $R_I = 5.9\%$; B, 8.8(2) Å^2 for Li(1), Cs(1), Cs(2), and Li(2) and 5.2(6) Å^2 for C_{60}. Data for Li_2CsC_{60} at 50 K are as follows: cell constants, 13.9889(12) Å; C_{60} shell radius, 3.555(4) Å; cubic harmonic coefficients, $C_{0,1} = 1.0$, $C_{6,1} = 0.05(1)$, $C_{10,1} = -0.16(3)$; R factors, $R_{wp} = 13.3\%$, $R_{exp} = 5.6\%$, $R_I = 7.7\%$; B, 6.2(2) Å^2 for Li(1) to C_{60}.

Atom	Site	*x*	*y*	*z*	*N*
		Room temperature			
Li(1)	8c	1/4	1/4	1/4	7.54(2)
Cs(1)	8c	1/4	1/4	1/4	0.46(2)
Cs(2)	4b	1/2	1/2	1/2	3.54(2)
Li(2)	4b	1/2	1/2	1/2	0.46(2)
C_{60}	4a	0	0	0	240
		50 K			
Li(1)	8c	1/4	1/4	1/4	7.59(2)
Cs(1)	8c	1/4	1/4	1/4	0.41(2)
Cs(2)	4b	1/2	1/2	1/2	3.59(2)
Li(2)	4b	1/2	1/2	1/2	0.41(2)
C_{60}	4a	0	0	0	240

Steric factors should also contribute to the stability of this novel orientational state of the fullerene units that usually tended in the solid state to align their hexagonal faces (and molecular threefold symmetry axes) along the $\langle 111 \rangle$ crystal directions. An orientational distribution function similar to pristine C_{60} would have led to a large coordination number for the tetrahedral ions and steric crowding for the small Li^+ ions. Our present results are thus consistent with the trend of decreasing coordination number of the tetrahedral ions in fulleride solids with decreasing ionic size (*2*). When the ionic radius of the alkali A^+ ion is larger than the size of the tetrahedral interstices (~1.12 Å), then A is K or Rb, the repulsive A^+–C interactions dominate the orientational potential, and the C_{60} ions present eight hexagonal faces to the tetrahedral sites, resulting in a coordination number of 24. However, when $r_{A^+} < 1.12$ Å (A = Na), the repulsive A^+–C interaction is substantially diminished (*21*), leading to an optimal A^+–C_{60} coordination, in which each $C_{60}{}^{3-}$ ion presents two hexagonal faces and six hexagon-hexagon fusions to its eight neighboring A^+ ions, reducing the coordination number from 24 to 12 (*2, 22*).

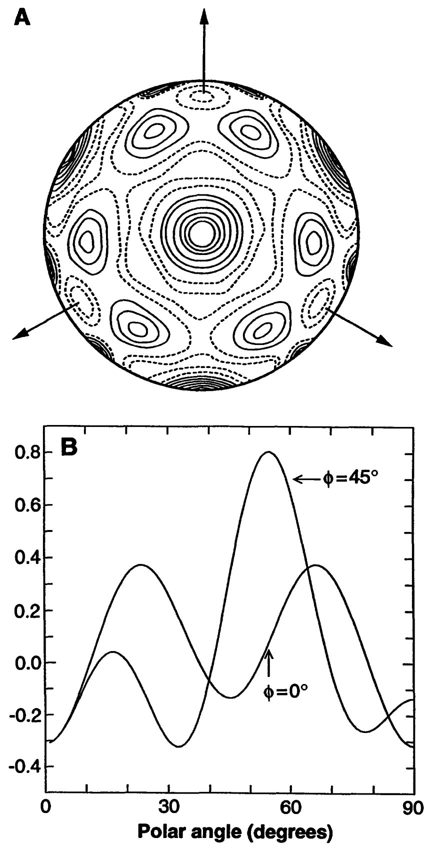

Fig. 3. (**A**) The orientation distribution function for C_{60} in Li_2CsC_{60} at room temperature viewed down one of the $\langle 111 \rangle$ directions. The zero-order term is omitted to emphasize differences from spherical symmetry. Solid and dashed contours indicate excess and deficit, respectively, carbon density with respect to the zero-order term. Contour intervals are ±0.128. (**B**) Cuts through the spherical surface plot of (A) along constant azimuthal angles, $\phi = 45°$ {[1$\bar{1}$0] plane} and 0° {[100] plane} showing the orientational density as a function of polar angle θ.

The nature (static, dynamic, or both) of orientational disorder present in Li_2CsC_{60} is difficult to decipher from the present results, as x-ray diffraction probes the time-averaged molecular and crystal structure and additional experiments with dynamical probes (^7Li and ^{13}C nuclear magnetic resonance quasielastic and inelastic neutron-scattering measurements, for example) are needed. However, large isotropic temperature factors persist to low temperatures both for the spherical shell and the alkali ions, indicating the existence of some static disorder (Table 1).

The fcc, merohedrally disordered, superconducting $A_2A'C_{60}$ compounds obey a simple monotonic relation (*6*) between T_c and the lattice constant a. This relation has been attributed to the interfullerene spacing modulating the electronic density of states at the Fermi level. A similar relation has been also proposed for orientationally ordered primitive cubic fullerides, with T_c showing a steeper dependence on intermolecular distance than in the fcc systems (*2*). The present structural characterization of fcc Li_2CsC_{60}, in which C_{60} adopts a different orientational state with dramatic effects on the macroscopic properties, now adds an additional dimension in the role of orientational disorder on the superconducting properties of the fullerides. The Li_2CsC_{60} fulleride is not superconducting, although the transition temperatures expected for the value of its lattice constant should be on the order of ~5 to 10 K. The detrimental effect on superconductivity should come from the strong lithium-carbon interaction that modifies the electronic structure at the Fermi level through hybridization. In addition, electron hopping between neighboring molecules may be adversely affected by the quasispherical disordered state of the fulleride ions.

High-resolution x-ray diffraction has been used to show the existence of a third possible structural modification of alkali fullerides with stoichiometry of $A_2A'C_{60}$, realized for the small dopant, A = Li^+ cation. The combination of small size and weak electropositive character for lithium leads to the formation of an fcc phase, incorporating quasispherical fulleride ions and characterized by bonding lithium-carbon interactions. Detailed band structure calculations are needed to explore the exact origin of the nonappearance of superconductivity in this phase, despite the apparent correct band filling and suitable interfullerene spacing. It appears that the orientational state of the fullerenes and the intercalate-carbon interaction subtly control the pair-binding mechanism in the fullerides.

REFERENCES AND NOTES

1. P. W. Stephens *et al.*, *Nature* **351**, 632 (1991).
2. K. Prassides *et al.*, *Science* **263**, 950 (1994).
3. K. Kniaz *et al.*, *Solid State Commun.* **88**, 47 (1993).
4. S. Chakravarty, M. P. Gelfand, S. Kivelson, *Science* **254**, 970 (1991).
5. C. M. Varma *et al.*, *ibid.*, p. 989; M. Schluter *et al.*, *Phys. Rev. Lett.* **68**, 526 (1992); I. I. Mazin *et al.*, *Phys. Rev. B* **45**, 5114 (1992).
6. R. M. Fleming *et al.*, *Nature* **352**, 787 (1991).
7. S. Satpathy *et al.*, *Phys. Rev. B* **46**, 1773 (1992); M. P. Gelfand and J. P. Lu, *ibid.*, p. 4367; *Appl. Phys. A* **56**, 215 (1993); T. Yildirim, S. Hong, A. B. Harris, E. J. Mele, *Phys. Rev. B* **48**, 12262 (1993); R. P. Gupta and M. Gupta, *ibid.* **47**, 11635 (1993).
8. K. Tanigaki *et al.*, *Europhys. Lett.* **23**, 57 (1993).
9. P. C. Chow *et al.*, *Phys. Rev. Lett.* **69**, 2943 (1992).
10. W. N. Setzer and P. von R. Schleyer, *Adv. Organomet. Chem.* **24**, 553 (1985).
11. J. E. Fischer, in *Intercalated Layered Materials*, F. Lévy, Ed. (Reidel, Dordrecht, Netherlands, 1979), pp. 481–532.
12. Li_2CsC_{60} samples were synthesized by direct reaction between C_{60} and alkali metals. Stoichiometric amounts of C_{60}, Li, and Cs were introduced into tantalum cells that were sealed in pyrex glass tubes filled with helium to 500 torr. These tubes were heated at 230°C for 12 to 24 hours and then baked at 430°C for 2 to 3 weeks. Susceptibility measurements were performed to 50 mK with a dilution refrigerator. DSC measurements were performed with a Mettler (Hightstown, NJ) DSC 3000 calorimeter on 10 to 30 mg of sample, sealed in aluminum pans. Measurements were carried out in the temperature range of 100 to 450 K at rates of 5 and 10 K/min.
13. PROFIL, 5.12; J. K. Cockcroft, Birkbeck College, London.
14. K. Tanigaki *et al.*, *Phys. Rev. B*, in press.
15. H. B. Bürgi, R. Restori, D. Schwarzenback, *Acta Crystallogr. B* **49**, 832 (1993); K. Rapcewicz and J. Przystawa, *Phys. Rev. B*, in press.
16. W. Press and A. Hüller, *Acta Crystallogr. A* **29**, 252 (1973); J. P. Amoureux and M. Bee, *Acta Crystallogr. B* **36**, 2636 (1980); J. K. Cockcroft and A. N. Fitch, *Z. Kristallogr.* **184**, 123 (1988).
17. For spherical-shell scatterers, the structure factor is the Fourier transform of the convolution of the position of the center of the shell, **R**, the scattering density function $\rho(\mathbf{r})$ of the shell (with the origin for **r** at **R**), and its thermal motion, μ

$$F_{hkl} = F^{rot}(Q)\exp(i\mathbf{Q}\cdot\mathbf{R})\cdot\exp[-W(\mathbf{Q})] \quad (1)$$

where **Q** is the scattering vector, $W(\mathbf{Q})$ is the Debye-Wallerfactor, and the rotational form factor of the shell is given by

$$F^{rot}(Q) = \int_{\text{unit cell}} f(Q)\exp(i\mathbf{Q}\cdot\mathbf{R})\cdot\rho(\mathbf{r})d\mathbf{r} \quad (2)$$

where $f(Q)$ is the atomics scattering factor. The orientational scattering density, $\rho(\mathbf{r})$, is expressed in terms of the SASH functions $[K_{lv}(\theta,\phi)]$ obtained from linear combinations of spherical-harmonic functions $\{Y_{lm}(\theta,\phi)$ [F. C. von der Lage and H. A. Bethe, *Phys. Rev.* **71**, 612 (1947)]}, as

$$\rho(\mathbf{r}) = \sum_l\sum_v C_{lv}K_{lv}(\theta_r,\phi_r)\,\delta(r-R)/4\pi R^2 \quad (3)$$

where R is the radius of the shell and C_{lv} are refinable coefficients. Substitution into Eq.2 and use of the orthonormality of the SASH functions results in

$$F^{rot}(Q) = (4\pi)^{1/2}f_C(Q)\sum_l\sum_v i^l j_l(QR)\,C_{lv}K_{lv}(\theta_Q,\phi_Q) \quad (4)$$

where $j_l(QR)$ are the l-th order spherical Bessel functions and $f_C(Q)$ is the carbon scattering factor. Only the coefficients, C_{lv}, that transform as the totally symmetric representation of the point group of the site symmetry of the shell of atoms are nonzero. The integer v labels the particular representation within A_{lg} for a given value of l.
18. K. H. Michel, J. R. D. Copley, D. A. Neumann, *Phys. Rev. Lett.* **68**, 2929 (1992).
19. I. Hirosawa, J. Mizuki, K. Tanigaki, H. Kimura, *Solid State Commun.* **89**, 55 (1994).
20. We tested our procedure by refining a room temperature synchrotron x-ray diffraction profile of pristine C_{60}, collected at Brookhaven National Laboratory. Reliable cubic harmonic $C_{6,1}$ and $C_{10,1}$ coefficients were routinely extracted from the refinement and were in good agreement with the values deduced by Chow *et al.*, (*9*) from single-crystal data. We thank P. A. Heiney for making his raw data available to us [*J. Phys. Chem. Solids* **53**, 1333 (1992)].
21. T. Yildirim *et al.*, *Phys. Rev. Lett.* **71**, 1383 (1993).
22. C. Christides *et al.*, *Europhys. Lett.* **24**, 755 (1993).
23. We thank the Engineering and Physical Sciences Research Council, United Kingdom, for financial support and access to Daresbury Laboratory, and K. H. Michel for useful discussions. M.G. is a participant of the University of Sussex–University of Waterloo (Canada) student exchange programme.

3 March 1994; accepted 4 April 1994

Critical Behavior in the Satisfiability of Random Boolean Expressions

Scott Kirkpatrick and Bart Selman

Determining the satisfiability of randomly generated Boolean expressions with *k* variables per clause is a popular test for the performance of search algorithms in artificial intelligence and computer science. It is known that for $k = 2$, formulas are almost always satisfiable when the ratio of clauses to variables is less than 1; for ratios larger than 1, the formulas are almost never satisfiable. Similar sharp threshold behavior is observed for higher values of *k*. Finite-size scaling, a method from statistical physics, can be used to characterize size-dependent effects near the threshold. A relationship can be drawn between thresholds and computational complexity.

Properties of randomly generated combinatorial structures often exhibit sharp threshold phenomena. A good example can be found in random graphs. A graph is defined as a set of points (vertices) in space with lines (edges) connecting pairs of vertices. A random graph is generated by randomly selecting pairs of vertices to be connected by edges. Erdös and Rényi (*1*) showed that many properties of random graphs can be predicted with a very high accuracy. Consider the sizes of connected clusters. A connected cluster is a group of vertices where, starting at an arbitrary vertex, one can reach any other vertex in the group by traversing one or more edges in the graph. It is intuitively clear that the more edges in the graph, the more vertices will be interconnected and the larger the clusters will be. What is surprising is that gradually increasing connectivity leads to sudden changes in the distribution of cluster sizes.

Let N be the number of vertices and M be the number of edges. If we make N and M large but hold their ratio $\alpha \equiv M/N$ constant, then we can identify two regimes: When $\alpha < 1/2$, many small isolated clusters of maximum size $\ln N$ are found; when $\alpha > 1/2$, a single giant component with size proportional to N absorbs many of the clusters. At the boundary between the two regimes, when α has its critical value $\alpha_c = 1/2$, the largest clusters are proportional to $N^{2/3}$. Subsequent work (*2, 3*) has made precise the sharpness of the threshold: Its characteristics persist across a range of α of order $N^{-1/3}$ about $\alpha_c = 1/2$. This is now recognized as the prototype of "percolation" phase transitions studied in simple models of real inhomogeneous materials, which change sharply from nonconducting to conducting on macroscopic scales as a local measure of connectedness increases (*4*). We shall use this well-understood model to test techniques for the identification of critical phenomena in less understood combinatoric structures.

Threshold phenomena have recently been observed in randomly generated Boolean expressions or formulas. Mitchell *et al.* (*5*) considered the *k*-satisfiability problem (*k*-SAT). An instance of *k*-SAT is a Boolean formula in a special form, called conjunctive normal form (CNF). An example of such a formula is $(x \vee y) \wedge (\bar{x} \vee \bar{y}) \wedge (x \vee \bar{y})$, where x and y are Boolean variables and $\wedge$, $\vee$, and the overbar are logical operators denoting, respectively, AND, OR, and NOT.

Each Boolean variable can be assigned either true or false. Depending on the

S. Kirkpatrick, IBM Thomas J. Watson Research Center, Yorktown Heights, NY 10598, USA. E-mail: kirk@watson.ibm.com
B. Selman, AT&T Bell Laboratories, Murray Hill, NJ 07974, USA. E-mail: selman@research.att.com